

AMap: Distilling Future Priors for Ahead-Aware Online HD Map Construction

Ruikai Li^{1,2*}, Xinrun Li^{3*}, Mengwei Xie², Hao Shan¹,
 Shoumeng Qiu¹, Xinyuan Chang², Yizhe Fan¹, Feng Xiong², Han Jiang¹,
 Yilong Ren¹, Haiyang Yu¹, Mu Xu², Yang Long⁴, Varun Ojha³, Zhiyong Cui^{1†}

¹ State Key Lab of Intelligent Transportation System, China ² Amap, Alibaba Group, China
³ Newcastle University, England ⁴ Durham University, England

*Equal contribution

†Corresponding author

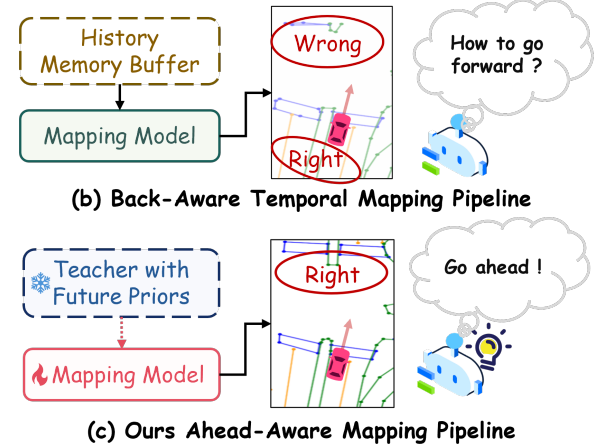
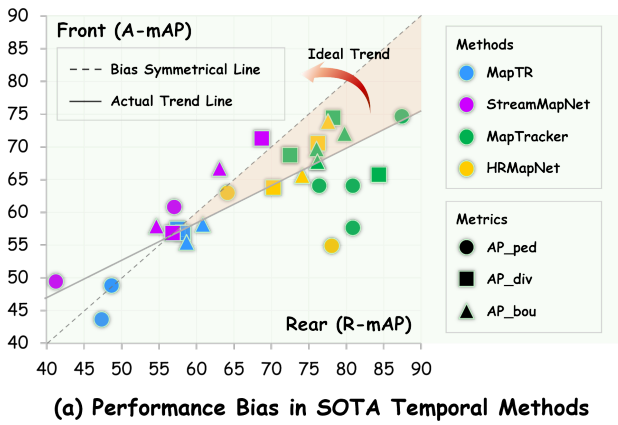


Figure 1. (a) **Performance Bias in SOTA Temporal Methods.** Current state-of-the-art temporal mapping methods exhibit a severely weaker mAP in front region (A-mAP) than it in rear views (R-mAP), as illustrated in the orange-shaded region. (b) & (c) **Back-Aware Pipeline vs. Our Ahead-aware Pipeline.** While the (b) Back-Aware mapping paradigm enhances perception in the vehicle’s rearward area, this comes at the cost of limited gains in forward spatial awareness. In contrast, our paradigm (c) effectively achieves forward perception gains by acquiring future priors through knowledge distillation.

Abstract

Online High-Definition (HD) map construction is pivotal for autonomous driving. While recent approaches leverage historical temporal fusion to improve performance, we identify a critical safety flaw in this paradigm: it is inherently “spatially backward-looking.” These methods predominantly enhance map reconstruction in traversed areas, offering minimal improvement for the unseen road ahead. Crucially, our analysis of downstream planning tasks reveals a severe asymmetry: while rearward perception errors are often tolerable, inaccuracies in the forward region directly precipitate hazardous driving maneuvers. To bridge this safety gap, we propose AMap, a novel framework for Ahead-aware online HD Mapping. We pioneer a “distill-from-future” paradigm, where a teacher model with privileged access to future temporal contexts guides a lightweight student model restricted to the current frame. This process implicitly compresses prospective knowledge into the student model, endowing it with “look-

ahead” capabilities at zero inference-time cost. Technically, we introduce a Multi-Level BEV Distillation strategy with spatial masking and an Asymmetric Query Adaptation module to effectively transfer future-aware representations to the student’s static queries. Extensive experiments on the nuScenes and Argoverse 2 benchmark demonstrate that AMap significantly enhances current-frame perception. Most notably, it outperforms state-of-the-art temporal models in critical forward regions while maintaining the efficiency of single current frame inference.

1. Introduction

HD Map is indispensable for autonomous driving systems, providing precise and stable semantic representations of static environments. However, traditional offline HD map is plagued by high costs and poor scalability. To overcome these limitations, recent research has spurred the development of online HD mapping techniques [6, 18, 23, 25, 27, 29, 32, 45, 48]. These methods seek to infer vectorized representations of map elements directly and in real-time from

the vehicle’s onboard sensory data, and have demonstrated promising performance in complex autonomous driving scenarios. A prevailing trend among state-of-the-art online mapping methods is the integration of historical temporal information [4, 19, 22, 42, 43]. By processing sequential data, these approaches leverage historical context to enhance the perception of the current frame. This effectively mitigates current-frame limitations, such as occlusion, to yield more consistent and complete map outputs.

Nevertheless, this reliance on historical data introduces a critical and largely unaddressed flaw: “backward-looking” bias, as illustrated in Fig. 1 (a) and (b). Through a detailed analysis of existing state-of-the-art temporal models on the nuScenes [1] benchmark, we find that their performance gains are not uniform. To quantify this, we introduce a novel ahead-aware evaluation metric (see Sec. 4.1). Our analysis reveals a stark asymmetry: the temporal fusion primarily enhances perception accuracy in areas where the ego-vehicle has already traversed, while its capability in the critical, unseen road ahead remains largely unimproved.

This performance bias creates a fundamental mismatch with an autonomous driving system’s operational priorities. Planning and decision-making systems rely far more critically on an accurate understanding of the upcoming road geometry than on areas already passed. Our preliminary experiments further illuminate this: we observe that masking out the rearward perception output often leads to a less severe degradation in downstream planning performance, and in some cases, even a slight improvement, compared to masking out the forward perception. This stark contrast underscores the differential importance of accurate perception in these distinct regions. Such findings lead us to a critical research question: *Is it feasible to design a lightweight, plug-and-play module to eliminate the forward-perception deficit without requiring additional architectural changes or inference cost?*

To bridge this gap, we propose AMap, a novel Ahead-aware Mapping framework based on knowledge distillation. Our core insight is to leverage future priors, which are readily available during the training phase, as a powerful supervisory signal to guide a standard current-frame (online) model. As illustrated in Fig. 1 (c), we employ a “distill from the future” strategy. We first train a powerful teacher model that incorporates future temporal context. Then, we distill its informative, future-aware representations into a lightweight student model that is restricted to only the current frame at inference. This process implicitly compresses prospective knowledge into the student, endowing it with a “look-ahead” capability without processing any future (or even historical) frames during deployment.

This distillation task, however, presents unique challenges. Standard distillation methods are not directly applicable, particularly for the dynamic, set-based predictions

of vectorized mapping. The student (online) and teacher (future-aware) models operate on different contexts, creating an “asymmetric” setting for distillation, especially at the query-decoder level. To address this, we introduce three technical components: Bird’s Eye View (BEV) masking, multi-level BEV feature distillation, and query matching transfer to effectively transfer knowledge from the teacher’s decoder to the student, despite the contextual asymmetry. Our principal contributions are threefold:

- We are the first to identify and systematically analyze the “backward-looking” flaw in current temporal-fusion mappers. To quantify this, we introduce a new benchmark and a novel forward-aware metric designed to evaluate perception accuracy in the critical, unseen areas ahead of the vehicle.
- We propose AMap, a novel ahead-aware knowledge distillation framework that pioneers a “distill-from-future” paradigm. By leveraging a teacher model with privileged access to future temporal contexts, we explicitly transfer prospective knowledge into a current-frame student. This endows the model with “look-ahead” capabilities at zero inference-time cost, supported by our proposed BEV masking, multi-level BEV feature distillation, and query matching transfer modules.
- Comprehensive evaluations on the nuScenes [1] and Argoverse 2 [38] benchmark demonstrate that our approach markedly improves the perceptual accuracy of the current-frame model, particularly in critical forward areas. Impressively, it outperforms several advanced temporal models in frontal perception accuracy while maintaining the efficiency of single current frame inference.

2. Related Work

Online HD Map Construction. While indispensable for autonomous driving, traditional HD maps suffer from high costs and an inability to handle dynamic scenes, motivating the development of online mapping techniques. Early online methods [13, 18, 28, 31] centered on generating BEV semantic maps. However, this resulted in suboptimal pixel output for downstream planning. This limitation was overcome by subsequent end-to-end vectorized paradigms [3, 6, 7, 9, 22, 23, 25–27, 29, 33–36, 39–41, 44, 45, 47, 48], which produce structured, instance-level map elements for immediate use. The frontier of research now lies in exploiting temporal information, where the integration of historical frames has led to state-of-the-art accuracy by enforcing temporal consistency [4, 19, 22, 42, 43]. However, these temporal fusion methods rely predominantly on historical information from areas in which the vehicle has already passed. Consequently, while they achieve impressive overall accuracy, the resulting performance gain offers limited improvement in perceiving the forward region, which is arguably more critical for planning and safety. Further-

more, the introduction of temporal fusion modules often brings substantial parameter increases and significant computational overhead, hindering real-time application. This paper addresses these limitations by introducing a novel distillation framework that leverages future priors to explicitly enhance ahead-aware perception. Our approach not only shifts the focus from a backward-looking to a forward-aware paradigm, but also achieves this without introducing any additional inference-time cost.

Knowledge Distillation. Knowledge Distillation (KD) compresses knowledge from a powerful teacher model into an efficient student model. This strategy is prevalent in autonomous driving perception, including 3D object detection [5, 15, 50, 51], online HD mapping [8], topology understanding [20], and 3D occupancy prediction [14, 46]. Typically, for information that is infeasible during deployment due to cost or latency, KD leverages it as privileged supervision to guide a lightweight student model via an implicit training-time transfer, thereby enhancing its capability without inference overhead. A canonical paradigm in this domain involves distilling cross-modal knowledge from a multi-modal teacher into a uni-modal student branch. Beyond modality transfer, KD also serves as a robust source of supervision in the form of pseudo-labels [24] or intermediate representations to facilitate model training [10]. In this work, we extend the application of KD to the temporal dimension. Specifically, we propose distilling knowledge from a teacher model that is privileged with future temporal information into an efficient student model, thereby instilling anticipatory perception capabilities for online mapping.

Temporal Modeling for Perception. Effective temporal modeling is crucial for a coherent and robust autonomous driving perception system. Existing methods can be broadly categorized by the temporal context they leverage. A dominant line of research focuses on historical information, integrating past sensor data to resolve perceptual ambiguities in the present frame. This approach, evident in BEV-based 3D object detection [12, 21] and online map construction [4, 43], primarily aims at enhancing temporal consistency, smoothing outputs, and mitigating occlusions by accumulating information from already-observed areas. In contrast, another body of work engages with future information, most prominently in the field of motion forecasting [16, 17, 37, 49]. Here, the goal is to anticipate the future states of dynamic agents, relying heavily on understanding their past trajectories and interactions. Our work introduces a novel perspective on temporal modeling by leveraging future information not for forecasting dynamic agents, but for enhancing the perception of the static environment itself. We demonstrate that future frames constitute a powerful source of privileged information for learning a more accurate and anticipatory representation of the road geometry, effectively addressing the spatial misalignment inherent in

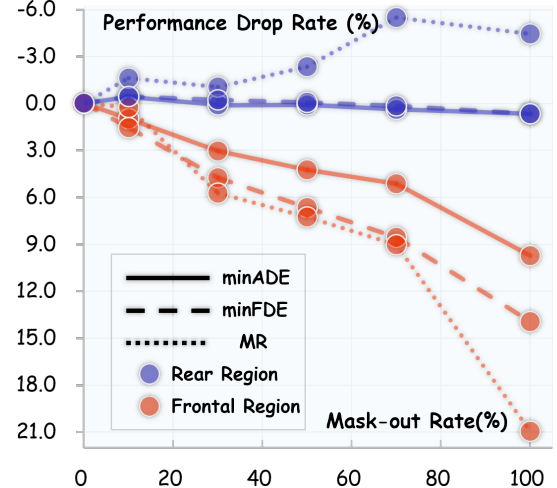


Figure 2. **Impact of directional masking the outputs of the online HD mapper on downstream trajectory prediction.** As the Forward Mask ratio increases (red line), metrics such as minADE, minFDE, and MR deteriorate significantly, whereas the Backward Mask (blue line) has negligible impact. This empirical evidence demonstrates that downstream tasks are critically dependent on the ahead-aware mapping outputs.

historical-fusion methods for online HD mapping.

3. Preliminary Experiments

To quantitatively assess how the performance of online mapping models in forward and backward spatial domains influences downstream tasks, we design a downstream task-driven evaluation framework. Our approach is motivated by findings from [49], which revealed that trajectory prediction accuracy is highly dependent on the quality of online maps. Building on this, we posit that if the contributions of forward and backward map regions to a downstream task are symmetric, then performance degradation in either region should yield comparable effects. In contrast, asymmetric impacts would indicate a spatial bias in the downstream model’s reliance on map information.

Table 1. **Downstream Sensitivity to Forward Degradation.**

Mask Ratio	Downstream Task Metric		
	minADE↓	minFDE↓	MR↓
-	0.3856	0.7919	0.0854
10%	0.3893 (+0.96%)	0.8040 (+1.53%)	0.0856 (+0.23%)
30%	0.3973 (+3.03%)	0.8296 (+4.76%)	0.0903 (+5.74%)
50%	0.4019 (+4.23%)	0.8446 (+6.65%)	0.0916 (+7.26%)
70%	0.4054 (+5.13%)	0.8595 (+8.54%)	0.0931 (+9.02%)
100%	0.4231 (+9.73%)	0.9024 (+13.95%)	0.1033 (+20.96%)

Experimental Setup. We adopt general MapTR [22] as our baseline. In its vectorized output maps, we systematically apply masking to the front and rear regions along the longitudinal axis of the ego vehicle, simulating controlled degradation in these spatial domains. Different masking ratios

Table 2. Downstream Sensitivity to Backward Degradation.

Mask Ratio	Downstream Task Metric		
	minADE \downarrow	minFDE \downarrow	MR \downarrow
-	0.3856	0.7919	0.0854
10%	0.3840 (-0.41%)	0.7884 (-0.44%)	0.0840 (-1.64%)
30%	0.3860 (+0.10%)	0.7901 (-0.23%)	0.0845 (-1.05%)
50%	0.3859 (+0.08%)	0.7913 (-0.08%)	0.0834 (-2.34%)
70%	0.3870 (+0.36%)	0.7932 (+0.16%)	0.0807 (-5.50%)
100%	0.3882 (+0.67%)	0.7971 (+0.66%)	0.0816 (-4.45%)

are applied to either forward or backward areas to emulate varying levels of map quality loss. The perturbed maps are then processed by a standard trajectory prediction model, HiVT [52], and evaluated using established metrics: Minimum Average Displacement Error (minADE), Minimum Final Displacement Error (minFDE), and Miss Rate (MR).

Experimental Analysis. As shown in Table 1, Table 2, and Fig. 2, our experimental results reveal a distinct asymmetry in how downstream tasks utilize online mapping information. Forward map regions are critical. Masking the forward area leads to a significant and monotonic degradation in all trajectory prediction metrics. When 100% of the forward region is masked, minADE increases by 9.73%, and minFDE increases by 13.95%. This strong correlation confirms that the quality of the forward map is a primary determinant of downstream performance. Backward map regions exert minimal influence on performance. In contrast, masking the backward region results in negligible or slightly positive changes; for instance, a 70% mask improves the Miss Rate (MR) from 0.0854 to 0.0807. This suggests that the high-fidelity details captured in these regions provide diminishing returns for future-oriented tasks, and that excessive precision can introduce noise, likely due to overfitting to irrelevant contextual details.

4. Methodology

4.1. Ahead-Aware Metric: A-mAP

Based on the analysis in Sec. 3, we observe a significant discrepancy in how map information from the forward and backward domains influences downstream task performance. However, most existing online mapping models focus primarily on overall map accuracy, lacking a dedicated metric to assess the precision of forward-facing map regions. To address this gap, we propose Ahead mAP (A-mAP), a downstream task-oriented evaluation metric that quantifies map construction quality specifically in the area ahead of the ego vehicle. Correspondingly, we introduce Rear mAP (R-mAP) to evaluate performance in the rear domain. Together, these metrics enable a clearer comparison of forward-backward performance bias across different HD map construction methods.

Metric Computation. The region of interest (ROI) is di-

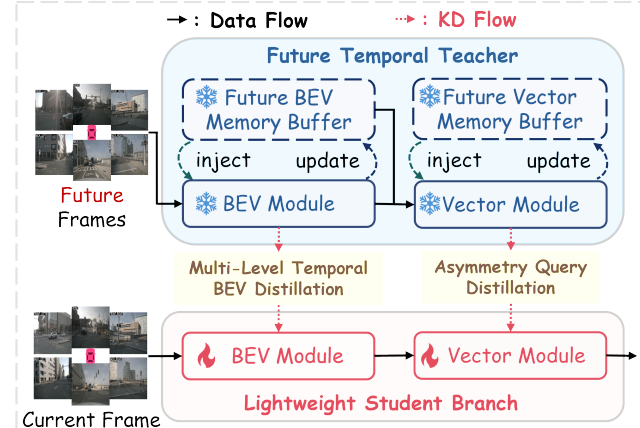


Figure 3. The overview of our proposed AMap framework.

vided into two halves relative to the ego vehicle’s heading: the area ahead and the rear area. The map construction quality metrics A-mAP and R-mAP are designed to evaluate the matching degree between predicted map elements and ground-truth elements within the ahead and rear regions, respectively. The computation process inside each half-region follows the same procedure as the global mAP, consisting of five stages: spatial alignment, vector matching, true positive identification, precision-recall calculation, and average precision computation. The detailed workflow is provided in the appendix.

4.2. AMap Framework

4.2.1. Model Overview

AMap is designed as a plug-and-play framework to bridge the performance gain bias in existing advanced temporal mapping models. It consists of a teacher model enriched with future temporal information and a lightweight student model, as illustrated in Figure 3. We elaborate the AMap framework in detail using a teacher-student model pair based on the MapTracker [4] codebase. Notably, the teacher model infused with future temporal information carries no physical significance during inference, since autonomous vehicles cannot access real future sensor inputs during operation. Instead, it serves solely as a privileged information carrier embedding forward-looking knowledge. The student model is a simplified current-frame variant of MapTracker, where temporal information is implicitly infused through knowledge distillation. Consequently, the student model acquires temporal awareness implicitly without introducing additional temporal or spatial overhead during inference. Note that AMap framework is also compatible with teacher models rich in historical information and can be coupled with various student architectures. To facilitate reader comprehension, “t” denotes the current frame, the subscript “T” indicates tensors of the teacher model, and the subscript “S” represents tensors of the student model.

Teacher with Future Priors. Our teacher model comprises

4 key components: the BEV Module, Future BEV Memory Buffer, Vector Module, and Future Vector Memory Buffer. Image features are extracted from multi-view RGB images through an image backbone. The BEV Module transforms the future BEV “memory” B^{t+1} to the current frame’s coordinate system based on pose information, after which the basic BEV features $B_T^{t,basic}$ of the current frame are obtained using spatial-deformable cross-attention similar to BEVFormer [21]. Furthermore, the 4 future “cached” BEV features from the Future BEV Memory Buffer are fused with the current features to derive refined BEV features $B_T^{t,refined}$. The refined BEV features are injected into the Future BEV Buffer while being passed to the Vector Module. The Vector Module first retrieves the query “memory” Q_T^{t+1} for the future $t+1$ frame from the Future Vector Memory Buffer and aligns it to the current frame via an MLP. The current frame’s queries are initialized as:

$$Q_T^{t,basic} = [Q_T^{t+1_{prop}}, Q_T^{t,new}], \quad (1)$$

where $Q_T^{t+1_{prop}}$ denotes “tracking” elements from the $t+1$ frame and $Q_T^{t,new}$ represents 100 new candidate queries. Subsequently, self-attention and BEV feature-based cross-attention are applied to enhance contextual representation. For each “tracking” element in the current frame, its corresponding future latent vector is selected from the Future Vector Memory Buffer for query fusion, yielding a refined query $Q_T^{t,refined}$. Finally, the filtered refined queries are fed into the detection head to produce the mapping results.

Lightweight Student. The lightweight current-frame student model is built upon the original MapTracker [4], with temporal fusion modules removed from both the BEV and Query dimensions. The base BEV features of the student branch $B_S^{t,basic}$ are obtained by transforming 2D image features, after which refined BEV features $B_S^{t,refined}$ are acquired through contextual enhancement. Due to the absence of a query buffer, the initialized learnable queries $Q_S^{t,new}$ are optimized via self-attention and BEV feature-based cross-attention. Similarly, prediction results of map elements are generated based on filtered high-confidence queries.

4.2.2. AMap Components

Multi-Level Temporal BEV Distillation. Following the paradigms established by BEVDistill [5] and MapDistill [8], we leverage knowledge distillation on BEV embeddings to transfer spatial-semantic information. However, distinct from previous approaches that primarily target the initial BEV features, we extend the distillation scope to the *refined* BEV representations, which are subsequently employed for the auxiliary segmentation task. We identify that applying global distillation directly to the entire feature map inevitably introduces background noise and leads to optimization imbalance due to the sparsity of foreground semantics. To mitigate this, we propose a ground-truth-guided

masking strategy. Specifically, we utilize the segmentation ground truth to generate a spatial mask \mathcal{M} , which suppresses irrelevant background signals and focuses the distillation on informative regions. The masked feature distillation loss is formulated as:

$$\mathcal{L}_{feat} = \frac{1}{\sum_{i,j} \mathcal{M}_{i,j}} \sum_{i=1}^H \sum_{j=1}^W \mathcal{M}_{i,j} \left\| \mathbf{F}_S^{(i,j)} - \mathbf{F}_T^{(i,j)} \right\|_2, \quad (2)$$

where $\mathbf{F}_T \in \mathbb{R}^{C \times H \times W}$ and $\mathbf{F}_S \in \mathbb{R}^{C \times H \times W}$ denote the basic and refined BEV feature maps from the teacher and student branches, respectively. $\mathcal{M}_{i,j} \in \{0, 1\}$ represents the binary mask derived from the segmentation ground truth, serving to spatially reweight the distillation loss.

Asymmetry Query Distillation. Distilling knowledge from time-series models that utilize dynamically tracked queries presents unique challenges, rendering conventional distillation techniques ill-suited. Methods demanding direct query-to-query alignment, such as MapDistill [8], are not directly applicable by this dynamic context. Moreover, our preliminary experiments confirmed that a naive approach is inherently limited in distilling a fixed set of static queries. To overcome this limitation, inspired by DETRDistill [2], we employ a matching-based dynamic query distillation strategy. This approach specifically addresses the problem of temporal query inconsistency inherent to models like MapTracker [4].

In detail, We first find one-to-one matching $\hat{\sigma}$ from the student’s N_S queries (e.g., 100) to the teacher’s N_T queries (e.g., 116) using the Hungarian algorithm. The logits distillation loss $\mathcal{L}_{logitsKD}$ is then computed only on these matched pairs:

$$\mathcal{L}_{logitsKD} = \sum_{i=1}^{N_S} \mathcal{L}_{KL} (\text{Logits}_S[i] \parallel \text{Logits}_T[\hat{\sigma}(i)]) \quad (3)$$

This formula sums the Kullback-Leibler divergence (\mathcal{L}_{KL}) over all N_S student queries. For each student query i , we distill its output $\text{Logits}_S[i]$ against the logits of the teacher query it was matched with, $\text{Logits}_T[\hat{\sigma}(i)]$. The mapping $\hat{\sigma}(i)$ provides the index of the specific teacher query that was optimally assigned to student query i .

5. Experiments

5.1. Experimental Settings

Dataset. The nuScenes [1] and Argoverse 2 [38] datasets are used to comprehensively evaluate the effectiveness of our approach. The nuScenes dataset contains 1,000 scene sequences, with keyframes annotated at 2 Hz. Each scene sequence consists of a 20-second video clip captured by 6 synchronized surrounding cameras. The Argoverse 2 dataset is recorded by 7 surrounding cameras and annotated at 10 Hz. The scene partitioning rules and the ground truth generation strategy follow previous work [4].

Table 3. Quantitative comparisons with non-KD camera-based online HD mapping models on the nuScenes validation set.

Method	Temporal	Backbone	AP _{p.} ↑	AP _{d.} ↑	AP _{b.} ↑	mAP↑	A-AP _{p.} ↑	A-AP _{d.} ↑	A-AP _{b.} ↑	A-mAP↑	R-mAP↑	FPS↑
MapTR (GKT)	✓	R50	45.99	53.39	54.46	51.28	43.64	54.89	58.14	52.23	55.22	14.7
MapTR (BEVFormer)	✓	R50	51.71	54.88	53.29	53.29	48.80	56.86	55.41	53.69	55.18	15.6
StreamMapNet	✓	R50	48.36	52.44	52.65	51.15	49.44	57.5	57.89	54.94	50.94	15.7
HRMapNet	✓	R50	62.46	64.81	66.33	64.53	57.63	63.79	65.61	62.34	69.51	16.2
MapTracker	✓	R18	71.68	67.25	69.09	69.34	64.06	68.75	67.76	66.86	76.51	22.3
MapTracker	✓	R50	72.73	75.77	70.31	72.93	74.66	65.75	69.69	70.03	78.92	15.6
MapTR	✗	R50	36.18	48.44	47.67	44.10	35.82	49.48	49.73	45.01	48.87	17.2
GeMap	✗	R50	45.62	53.95	54.20	51.26	41.37	56.91	56.56	51.61	54.74	13.7
MGMap	✗	R50	48.21	55.80	55.43	53.15	48.56	57.21	59.64	55.13	56.78	12.4
MapTRv2	✗	R50	60.18	61.33	62.62	61.38	60.42	64.78	67.44	64.21	61.82	14.4
MapQR	✗	R50	63.36	68.03	67.67	66.35	62.47	71.20	71.47	68.38	65.59	12.4
MapTracker	✗	R50	68.21	69.71	67.00	68.30	64.33	73.25	69.83	69.30	69.47	20.1
AMap (Ours)	✗	R50	69.97	70.13	67.67	69.26	65.09	74.48	71.01	70.19	69.61	20.1
MapTR	✗	R18	26.06	33.68	37.32	32.35	29.84	37.06	42.11	36.34	32.76	31.4
MapTRv2	✗	R18	54.07	59.12	58.25	57.15	56.69	62.10	63.65	60.81	56.17	16.6
MapQR	✗	R18	59.33	63.26	64.35	62.31	60.03	66.09	67.98	64.70	63.13	13.7
MapTracker	✗	R18	61.01	65.28	62.14	62.81	59.33	69.33	65.23	64.63	64.04	31.5
AMap (Ours)	✗	R18	63.11	67.08	63.27	64.49	60.70	71.96	66.16	66.28	65.11	31.5

• AP_{p.}, AP_{d.}, AP_{b.} denote the Average Precision (AP) for pedestrian crossings, lane dividers, and road boundaries, respectively.

Table 4. Quantitative comparisons with Other KD methods on the nuScenes validation set.

Distillation Setup	Setting	Method	Temporal	Backbone	AP _{p.} ↑	AP _{d.} ↑	AP _{b.} ↑	mAP↑	A-mAP↑	R-mAP↑
Future → Static	T	MapTracker	5 Future	R50	77.00	75.65	75.53	76.06	79.86	73.32
	S	MapTracker	None	R18	61.01	65.28	62.14	62.81	64.63	64.04
	KD	BEVDistill*	None	R18	56.33	60.75	56.82	57.97 (-4.84)	60.08 (-4.55)	60.06
	KD	MapDistill*	None	R18	57.08	59.60	56.78	57.82 (-5.61)	59.97 (-4.66)	59.87
	KD	AMap (Ours)	None	R18	63.11	67.08	63.27	64.49 (+1.68)	66.28 (+1.65)	65.11
Past → Static	T	MapTracker	5 Past	R50	72.73	75.77	70.31	72.93	70.03	78.92
	S	MapTracker	None	R18	61.01	65.28	62.14	62.81	64.63	64.04
	KD	BEVDistill*	None	R18	54.48	58.47	55.49	56.15 (-6.66)	58.47	58.86
	KD	MapDistill*	None	R18	56.03	59.53	57.32	57.63 (-5.18)	59.72	59.83
	KD	AMap (Ours)	None	R18	62.72	65.92	62.26	63.63 (+0.82)	65.08	65.08
Past → Past	T	MapTracker	5 Past	R50	72.73	75.77	70.31	72.93	70.03	78.92
	S	MapTracker	5 Past	R18	71.68	67.25	69.09	69.34	66.86	76.51
	KD	BEVDistill*	5 Past	R18	70.29	68.95	68.70	69.31 (-0.03)	65.91	76.69
	KD	MapDistill*	5 Past	R18	67.85	67.61	67.77	67.74 (-1.6)	64.75	75.00
	KD	AMap (Ours)	5 Past	R18	71.65	68.96	70.51	70.37 (+1.03)	65.99	79.95

• The table compares different temporal distillation settings.

• Future → Static: Distilling future frames into a static student. Past → Static: Distilling history into a static student.

• *: Temporal distillation completion version.

Evaluation Metric. Both the classic global metric mAP and our proposed A-mAP and R-mAP are employed to comprehensively evaluate previous works and our AMap framework. Following established protocols, we consider three map element categories: pedestrian crossing, lane divider, and road boundary.

Training. The training consists of two stages: teacher model pre-training and joint teacher-student training. During the joint teacher-student training phase, the teacher model parameters loaded from the pre-trained weights are entirely frozen, and only the student model parameters are updated. For the teacher model, we follow the default settings of MapTracker, where the temporal sampling strategy involves randomly selecting 4 frames from 10 consecutive

frames in chronological order. We use the AdamW [30] optimizer with an initial learning rate of 5e-4 and weight decay of 0.01. A cosine learning rate scheduler is employed, decaying to a final learning rate of 1.5e-6. All models are trained on 8 NVIDIA H20 GPUs.

5.2. Comparisons with State-of-the-art Methods

Benchmark and Analysis. To comprehensively evaluate the performance of existing online HD map construction methods in the front and rear spatial domains, we conduct a systematic assessment of current state-of-the-art camera-based methods on the nuScenes [1] validation set. As shown in Table 3, temporal models [4, 22, 43, 47] demonstrate a clear advantage in global performance metrics. How-

ever, most of them exhibit a notable asymmetry between the gains in A-mAP and R-mAP. For instance, MapTracker shows a large performance gap exceeding 8 points under both ResNet-18 and ResNet-50 backbones. This bias suggests that the performance gains of most existing temporal models primarily stem from improvements in the rear region, while a performance bottleneck remains in the forward area, which is more critical for downstream tasks.

In contrast, current-frame models [22, 23, 25, 29, 48] achieve a more balanced improvement between forward and rear metrics. Our proposed AMap distillation framework is designed to transfer forward-aware knowledge, embedded in a teacher model with future temporal priors, to a lightweight current-frame student model via knowledge distillation. Experimental results in Table 3 show that the AMap framework effectively improves mAP, A-mAP, and R-mAP without introducing extra inference cost. It is worth emphasizing that, unlike other temporal models that tend to boost rear region performance, the implicit injection of future temporal priors in AMap leads to a distinct gain in forward spatial perception.

Comparison with Other Knowledge Distillation Methods. Previous knowledge distillation approaches in autonomous driving have predominantly focused on cross-modal knowledge transfer. As summarized in Table 4, we design 3 comparative distillation settings: (1) distillation from a teacher model with future temporal information to a current-frame student model; (2) distillation from a teacher with past temporal information to a current-frame student; and (3) distillation from a teacher with past temporal inputs to a lightweight student that also incorporates historical information.

These 3 configurations demonstrate the superiority of our AMap distillation framework in temporally-aware distillation. Existing methods such as BEVDistill [5], and MapDistill [8], are generally designed for current-frame to current-frame knowledge transfer, making them less suitable for distilling temporal knowledge into a current-frame model. The stronger performance observed in the third group further confirms that distillation is more effective when the teacher and student operate under aligned temporal receptive fields, as compared to the asymmetric settings in groups “Future → Static” and “Past → Static”.

Table 5. Results based on the MapTR model.

Setting	Tem.	Back.	mAP \uparrow	A-mAP \uparrow	R-mAP \uparrow
Teacher	5 Future	R50	51.85	57.01	50.12
Baseline	\times	R18	32.35	36.34	32.76
+ Ours	\times	R18	47.84	51.29(+14.95)	47.59

5.3. Experiments on Generalization

Experiments on the MapTR model. The proposed AMap distillation framework is integrated into the MapTR [22]

Table 6. Results on the Argoverse2 validation set.

Method	Tem.	Back.	mAP \uparrow	A-mAP \uparrow	R-mAP \uparrow
MapTracker	5 past	R50	76.87	73.00	83.82
MapTracker	5 future	R50	75.57	80.79	72.42
MapTracker	None	R18	63.69	65.29	66.10
+ Ours	None	R18	65.25	67.81	67.53

architecture. The teacher model is built upon a ResNet-50 backbone and incorporates future temporal information, while the student model employs a lightweight ResNet-18 backbone and uses only current-frame input. As shown in Table 5, experimental results demonstrate that the student model equipped with the AMap distillation strategy achieves significant performance improvements compared to the baseline student model, even approaching the performance level of the teacher model. This validates the strong plug-and-play capability of the AMap framework.

Evaluation on Argoverse 2 Dataset. As shown in Table 6, the AMap distillation framework also demonstrates strong performance on the Argoverse 2 dataset [38]. Compared to the baseline student model, the student model equipped with our AMap distillation strategy achieves consistent improvements across all three evaluation metrics, including mAP, A-mAP and R-mAP. Particularly noteworthy is the significant performance gain of 2.52 A-mAP observed in the forward perception region.

Table 7. Effect of key designs in AMap.

BEV Level Basic	BEV Level Refined	Query Level	mAP \uparrow	A-mAP \uparrow	R-mAP \uparrow
\times	\times	\times	62.81	64.63	64.04
✓	\times	\times	62.66	64.33	64.31
\times	✓	\times	62.72	64.68	64.78
✓	✓	\times	63.47	65.20	65.54
\times	\times	✓	63.57	64.61	64.91
✓	✓	✓	64.49	66.28	65.11

Table 8. Impact of Asymmetry Query Distillation.

Method	AP _{p.} \uparrow	AP _{d.} \uparrow	AP _{b.} \uparrow	mAP \uparrow
baseline	61.01	65.28	62.14	62.81
+ BEV Level	62.49	65.18	62.09	63.25
+ MapDistill (dummy)	56.03	59.53	57.32	57.63
+ MapDistill (Top K)	53.55	58.86	57.42	56.61
+ Hungarian (MSE)	62.46	64.24	62.26	62.99
+ Hungarian (Cosine)	60.99	65.02	61.27	62.43
+ Ours	62.72	65.92	62.26	63.63

5.4. Ablation Study

Ablation study of core components in AMap. As shown in Table 7, we analyze our proposed BEV-level and query-level distillation strategies through different combinations. Comparing the first three ablation groups, we observe that employing a single BEV-level distillation strategy has limited impact on map construction accuracy. However, when both the refined and basic BEV features are used as loss

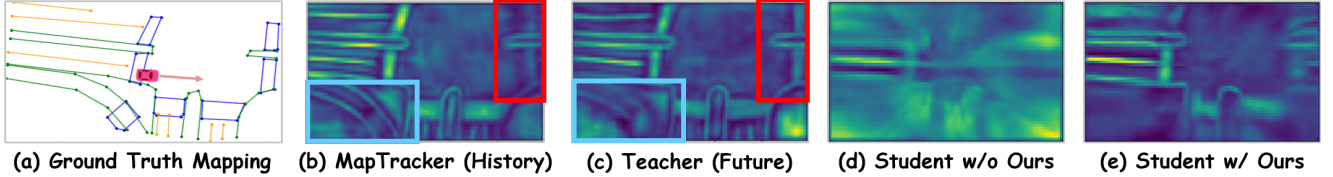


Figure 4. BEV feature visualization comparison among: (b) historical sequence-based MapTracker, (c) our teacher model with future priors, (d) the baseline student model, and (e) the student model with our proposed distillation strategy. Blue boxes and red boxes indicate the advantages of historical sequences and future sequences, respectively.

terms, the student model achieves noticeable improvement. Furthermore, we find that the two half-region metrics, A-mAP and R-mAP, are not strictly correlated with the global mAP. For instance, when only the refined BEV feature is used for supervision, both A-mAP and R-mAP increase to varying degrees, while the overall mAP decreases. We hypothesize that this phenomenon may be related to the region-splitting strategy; a detailed analysis is provided in the appendix. Additionally, we demonstrate that combining query-level and BEV-level supervision maximizes the distillation gains, yielding the best overall performance.

Ablation Study on Different methods for Asymmetry Query Distillation. As shown in Table 8, we ablate different distillation matching strategies on this asymmetry query problem. The baseline model achieves 63.25 mAP. Naive matching strategies, such as MapDistill [8] applied only on dummy queries or Top-K (K=100) queries in Maptracker [4], fail to establish proper student-teacher correspondence and cause a severe performance collapse, dropping to 57.63 and 56.61 mAP, respectively. We then evaluate more advanced assignment methods. Using Hungarian matching for assignment is sensitive to the loss function and fail to get performance gain when distill query embeddings: Hungarian (Cosine) and Hungarian (MSE) both degrade performance. Finally, our method when apply this distillation on logits using KL loss achieving the highest scores overall mAP (63.63).

5.5. Qualitative Results

Visual Comparison of BEV Features. As illustrated in Fig. 4, the teacher model with future temporal priors and the historically-driven MapTracker exhibit complementary strengths in scene representation: MapTracker (b) demonstrates stronger representational capacity in the rear spatial region, while the teacher model (c) achieves more discriminative scene perception ahead of the ego vehicle. Compared to the baseline student model (d), the BEV features of our AMap-enhanced student model (e) show significant improvement.

Visual Comparison in Complex Intersection Scenarios. As shown in Fig. 5, the student model enhanced with AMap distillation demonstrates significantly stronger ahead-aware mapping capability compared to the baseline student model. This advantage is particularly evident in its accurate recon-

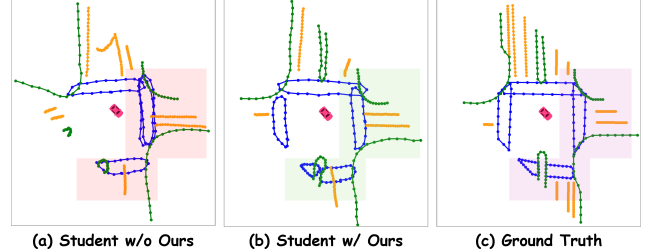


Figure 5. Qualitative results of the baseline student model (a), AMap (Ours) (b), and Ground-Truth (c).

struction of map elements such as pedestrian crossings and lane dividers in the forward driving direction, as well as all three categories of map elements at intersections to the right of the ego vehicle.

6. Conclusion

In this work, we have critically re-examined the prevailing temporal fusion paradigm in online HD map reconstruction and identified a severe “backward-looking” bias. Our investigation into downstream trajectory prediction tasks reveals a counter-intuitive but pivotal insight: high-precision reconstruction of the rearward environment is not only redundant but potentially distracting; notably, masking out rearward perception can surprisingly improve trajectory prediction performance. This highlights a fundamental misalignment between standard global mAP metrics and the decision-centric priorities of autonomous driving.

To resolve this, we proposed AMap, a novel framework that pioneers a “distill-from-future” mechanism. By treating future temporal context as privileged information, we successfully transfer “look-ahead” capabilities to a current-frame student. Our method achieves remarkable results: using a lightweight ResNet-18 backbone, AMap establishes a new state-of-the-art for forward-region perception. Crucially, it outperforms both historical distillation baselines and computationally heavy temporal models in the critical frontal view, even when the latter exhibit higher overall mAP due to their rearward bias. We believe this work charts a new course for the field, encouraging the community to rethink training strategies that prioritize task-relevant foresight over uniform reconstruction for predictive scene understanding.

7. Acknowledgements

This work was supported in part by the Beijing Natural Science Foundation under Grant L243008, in part by the Shandong Provincial Natural Science Foundation under Grant ZR2024LZN010, in part by the National Natural Science Foundation of China (NSFC) under Grant 52441202, and in part by the National Key R&D Program of China under Grant 2024YFB43000303.

AMap: Distilling Future Priors for Ahead-Aware Online HD Map Construction

Supplementary Material

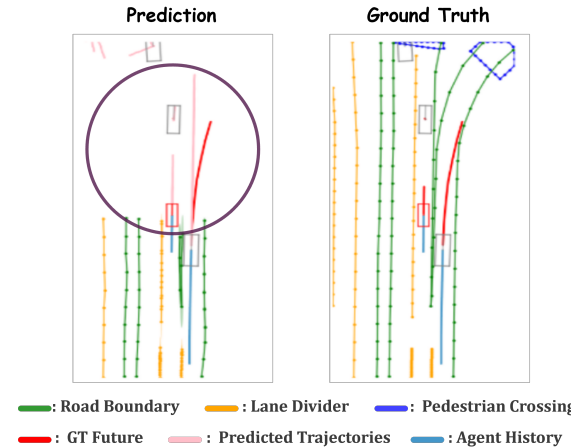


Figure 6. The visual impact of inaccuracies in forward map elements on downstream tasks is demonstrated in the left subfigure. Due to the autonomous driving system’s failure to correctly construct the ramp elements ahead of the vehicle, the system subsequently generated a dangerous straight-path trajectory.

In the supplementary material, we provide additional details covering preliminary experiments and discussions, experimental results and analysis of the AMap distillation framework, visualizations, training and inference specifics (including computational costs), calculation details of the A-Map metric, and a more comprehensive Ahead-aware Online Mapping benchmark with related analysis. The supplementary material is organized as follows:

- Sec. 8 presents additional preliminary experiments and discussions to better illustrate the impact of ahead-aware mapping on downstream tasks.
- Sec. 9 includes further ablation studies and more detailed visual comparisons.
- Sec. 10 describes additional training and inference configurations, together with an analysis of computational costs.
- Sec. 11 offers an extended A-mAP vs R-mAP benchmark and corresponding analysis on single frame models.

8. Extended Preliminary Experiments

A key motivation behind the proposed AMap framework stems from our observation that map elements in front of the vehicle generally exert greater influence on downstream tasks, as illustrated in Figure 6. Consequently, preliminary experiments were conducted to qualitatively and quantitatively validate the significantly higher importance of forward map areas compared to rear areas for downstream performance. In the baseline work [49], the map elements around the vehicle predicted by the map builder [22, 23], along with the historical trajectory of the vehicle, are used

as inputs to the trajectory prediction model [52]. Building upon this, we investigate the impact of forward online mapping on downstream trajectory prediction. We apply masks to different regions of the predicted map to simulate degradation in the prediction of map elements across various areas. As shown in Table 9, Table 10, and Figure 7, the experimental results reveal a clear and critical finding: degradation in forward map regions significantly impairs the performance of the downstream task, whereas degradation in rear map regions has almost no effect. Moreover, masking certain rear map elements can even lead to improved performance in the downstream task.

Table 9. Downstream Sensitivity to Forward Degradation.

Mask Ratio	Downstream Task Metric		
	minADE \downarrow	minFDE \downarrow	MR \downarrow
-	0.3856	0.7919	0.0854
5%	0.3875 (+0.49%)	0.7998 (+1.00%)	0.0851 (-0.35%)
10%	0.3893 (+0.96%)	0.8040 (+1.53%)	0.0856 (+0.23%)
15%	0.3906 (+1.30%)	0.8099 (+2.27%)	0.0876 (+2.58%)
25%	0.3956 (+2.59%)	0.8246 (+4.12%)	0.0898 (+5.15%)
30%	0.3973 (+3.03%)	0.8296 (+4.76%)	0.0903 (+5.74%)
40%	0.4002 (+3.79%)	0.8395 (+6.01%)	0.0913 (+6.91%)
50%	0.4019 (+4.23%)	0.8446 (+6.65%)	0.0916 (+7.26%)
60%	0.4035 (+4.64%)	0.8525 (+7.65%)	0.0940 (+10.07%)
70%	0.4054 (+5.13%)	0.8595 (+8.54%)	0.0931 (+9.02%)
80%	0.4071 (+5.58%)	0.8637 (+9.07%)	0.0949 (+11.12%)
90%	0.4153 (+7.70%)	0.8835 (+11.57%)	0.1004 (+17.56%)
100%	0.4231 (+9.73%)	0.9024 (+13.95%)	0.1033 (+20.96%)

Table 10. Downstream Sensitivity to Backward Degradation.

Mask Ratio	Downstream Task Metric		
	minADE \downarrow	minFDE \downarrow	MR \downarrow
-	0.3856	0.7919	0.0854
5%	0.3843 (-0.34%)	0.7884 (-0.44%)	0.0845 (-1.05%)
10%	0.3840 (-0.41%)	0.7884 (-0.44%)	0.0840 (-1.64%)
15%	0.3849 (-0.18%)	0.7886 (-0.42%)	0.0838 (-1.87%)
25%	0.3850 (-0.16%)	0.7892 (-0.34%)	0.0840 (-1.64%)
30%	0.3860 (+0.10%)	0.7901 (-0.23%)	0.0845 (-1.05%)
40%	0.3864 (+0.21%)	0.7909 (-0.13%)	0.0836 (-2.11%)
50%	0.3859 (+0.08%)	0.7913 (-0.08%)	0.0834 (-2.34%)
60%	0.3855 (-0.03%)	0.7919 (-0.00%)	0.0827 (-3.16%)
70%	0.3870 (+0.36%)	0.7932 (+0.16%)	0.0807 (-5.50%)
80%	0.3880 (+0.62%)	0.7936 (+0.21%)	0.0805 (-5.74%)
90%	0.3889 (+0.86%)	0.7953 (+0.43%)	0.0809 (-5.27%)
100%	0.3882 (+0.67%)	0.7971 (+0.66%)	0.0816 (-4.45%)

9. Comprehensive Experiments and Qualitative Results

Ablation Study on BEV Level Distillation. Two sets of ablation studies on BEV-level distillation are presented in Table 11. In Group # 1, both teacher and student models

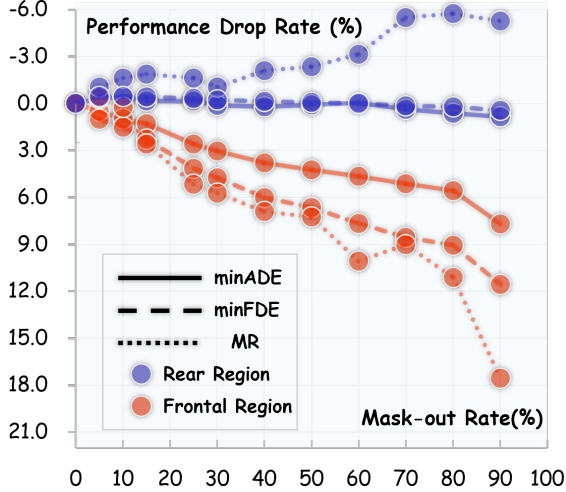


Figure 7. **Impact of directional masking the outputs of the online HD mapper on downstream trajectory prediction.** As the Forward Mask ratio increases (red line), metrics such as minADE, minFDE, and MR deteriorate significantly, whereas the Backward Mask (blue line) has negligible impact. This empirical evidence demonstrates that downstream tasks are critically dependent on the ahead-aware mapping outputs.

Table 11. **Impact of BEV Level Distillation.**

Group ID	Method	AP _{p.} ↑	AP _{d.} ↑	AP _{b.} ↑	mAP↑
Group # 1	baseline # 1	71.67	67.26	69.12	69.35
	+ BEV KD	68.96	71.45	68.89	69.76
	+ BEV Mask	70.76	70.07	69.25	70.03
Group # 2	baseline # 2	61.01	65.28	62.14	62.81
	+ BEV KD	61.53	65.39	61.34	62.76
	+ BEV Mask	62.49	65.18	62.09	63.25

are built upon the MapTracker [4] codebase with 5-frame historical temporal fusion. The key difference lies in the backbone: the teacher employs ResNet-50 [11], while the student uses ResNet-18 [11]. After applying basic BEV distillation, experimental results indicate performance degradation in two map element types (besides dividers) to varying degrees. We attribute this to differences in how map elements are represented in BEV feature space. Visualization of BEV features reveals that divider elements typically exhibit two characteristics: short length and longitudinal distribution, whereas crosswalk elements mostly appear as circular or transverse patterns, and boundary elements tend to be elongated. We hypothesize that the BEV representations of crosswalks and boundaries may introduce additional background noise during distillation, leading to performance degradation. To address this, we introduce a BEV mask that leverages ground truth map shapes to guide the student model to focus more on foreground representations while minimizing learning of background noise.

In Group # 2, the teacher model remains the ResNet-50-

based MapTracker with 5-frame temporal fusion, while the student model uses only the current frame with a ResNet-18 backbone. Compared to Group # 1, the crosswalk element performance in this group differs from the baseline. BEV feature visualizations suggest that temporally fused BEV representations contain slight noise along the lateral dimension, possibly due to the dependence of temporal fusion on vehicle pose information, which may introduce lateral errors and consequently affect BEV feature accuracy in that direction. Both experimental groups demonstrate that BEV distillation with masking can maximize student model performance by effectively preserving critical structural information while suppressing noise.

Additional Qualitative Experiments Results To visually demonstrate the effectiveness of our online map construction method, we conduct a qualitative visualization analysis on two autonomous driving benchmark datasets: nuScenes [1] and Argoverse 2 [38]. As Shown in Figure 9, Figure 10, and Figure 11, after applying our method, the quality of online map reconstruction in the forward region is significantly improved.

10. Details of Experiments

Training Loss. The overall loss function comprises two components: the basic loss $\mathcal{L}_{\text{basic}}$ computed against ground truth annotations, and a distillation loss derived from interaction with the teacher model. The basic loss $\mathcal{L}_{\text{basic}}$ follows the same configuration as standard MapTracker [4], including BEV loss \mathcal{L}_{BEV} , VEC loss \mathcal{L}_{VEC} , and Transformation loss $\mathcal{L}_{\text{trans}}$, which can be formally expressed as:

$$\mathcal{L}_{\text{basic}} = \mathcal{L}_{\text{BEV}} + \mathcal{L}_{\text{VEC}} + \mathcal{L}_{\text{trans}}. \quad (4)$$

For specific implementation details, please refer to the official settings of MapTracker [4].

The distillation loss consists of two parts: BEV feature loss $\mathcal{L}_{\text{feat}}$ and Asymmetric Query loss $\mathcal{L}_{\text{logitsKD}}$, formulated as:

$$\mathcal{L}_{\text{distill}} = \mathcal{L}_{\text{feat}} + \mathcal{L}_{\text{logitsKD}}. \quad (5)$$

The overall loss function can be formulated as:

$$\mathcal{L}_{\text{all}} = \mathcal{L}_{\text{basic}} + \mathcal{L}_{\text{distill}}. \quad (6)$$

Training Setting. All experiments were conducted on 8 NVIDIA H20 GPUs. Unlike MapTracker’s three-stage training paradigm (BEV pretrain, warm-up, and joint fine-tuning), the student model in AMap only undergoes the final training stage. We used a batch size of 16 and the AdamW optimizer with an initial learning rate of 5e-4. The training adopted a cosine learning rate scheduler with a final learning rate of 1.5e-6, and the weight decay was set to 0.01. In this work, we employ a consistent weighting scheme across all our experiments. Specifically, the weight for every loss term utilized throughout this paper is uniformly set to 1.0.

Table 12. **Computational efficiency.**

Method	Setting	Params \downarrow	Memory \downarrow	FPS \uparrow
baseline	Train	60.69 M	13.19 GB	-
baseline	Test	60.69 M	13.19 GB	31.5
baseline + Ours	Train	118.4 M	14.28 GB	-
baseline + Ours	Test	60.69 M	13.19 GB	31.5

Computational Efficiency. The computational overhead during training and inference is summarized in Table 12. While AMap incorporates additional parameters by loading the teacher model during training, this overhead can be mitigated by precomputing and caching intermediate tensors from the teacher model offline. During inference, the AMap framework achieves improved accuracy without introducing any additional computational cost.

11. Enhanced Benchmark Evaluation

We also benchmark the performance of various common single-frame models for online HDMap construction as shown in Table 13, including MapQR [29], GeMap [48], MapTRv2 [23], MGMap [25], and the single-frame variants of MapTR [22] and MapTracker [4], using the A-mAP and R-mAP metrics introduced in the main text. As illustrated in Fig 8, single-frame models do not suffer from the forward-perception deficit issue. Notably, a comparison between the single-frame and temporal variants (from main text) of MapTR and MapTracker clearly demonstrates that temporal aggregation introduces a significant bias towards superior performance in rear regions.

Table 13. Benchmark Results on the nuScenes validation set.

Method	Temporal	Backbone	BEV Encoder	Epoch	AP _{ped.} ↑	AP _{div.} ↑	AP _{bou.} ↑	mAP↑	A-AP _{ped.} ↑	A-AP _{div.} ↑	A-AP _{bou.} ↑	A-mAP↑	R-mAP↑
MapTR	✗	R18	GKT	24	26.06	33.68	37.32	32.35	29.84	37.06	42.11	36.34	32.76
	✗	R18	GKT	110	40.85	50.04	47.43	46.11	41.91	53.60	51.18	48.90	47.05
	✗	R50	GKT	24	36.18	48.44	47.67	44.10	35.82	49.48	49.73	45.01	48.87
	✗	R50	GKT	110	44.42	54.63	52.52	50.53	46.20	62.86	62.29	57.11	51.19
	✗	R50	BEVFormer	24	34.53	45.43	44.88	41.61	35.67	47.86	49.14	44.22	45.89
	✗	R50	BEVPool	24	44.96	51.86	53.48	50.10	46.80	56.69	58.61	54.03	46.30
	✓	R50	GKT	24	45.99	53.39	54.46	51.28	43.64	54.89	58.14	52.23	55.22
MapTRv2	✗	R50	BEVFormer	24	51.71	54.88	53.29	53.29	48.80	56.86	55.41	53.69	55.18
	✗	R18	BEVPool	24	54.07	59.12	58.25	57.15	56.69	62.10	63.65	60.81	56.17
MapQR	✗	R50	BEVPool	24	60.18	61.33	62.62	61.38	60.42	64.78	67.44	64.21	61.82
	✗	R18	BEVFormer	24	59.33	63.26	64.35	62.31	60.03	66.09	67.98	64.70	63.13
	✗	R50	BEVFormer	24	63.36	68.03	67.67	66.35	62.47	71.20	71.47	68.38	65.59
MGMap	✗	R50	BEVFormer	110	65.42	76.42	77.53	73.12	69.12	77.57	76.45	74.38	72.57
	✗	R50	BEVFormer	24	48.21	55.80	55.43	53.15	48.56	57.21	59.64	55.13	56.78
GeMap	✗	R50	BEVFormer	24	45.62	53.95	54.20	51.26	41.37	56.91	56.56	51.61	54.74
	✗	R50	BEVFormer	110	59.80	65.08	63.19	62.69	58.26	68.47	68.44	65.06	63.91
	✗	Swin-T	BEVFormer	110	70.43	72.77	72.76	71.99	69.89	75.24	76.18	73.77	72.79
	✗	V2-99	BEVFormer	110	70.18	72.19	73.70	72.02	68.97	75.16	76.44	73.52	72.66
	✗	V-99*	BEVFormer	110	74.28	75.99	77.68	75.99	72.70	78.00	80.24	76.98	76.36
HRMapNet	✗	R50	BEVFormer	24	62.46	64.81	66.33	64.54	57.63	63.79	65.61	62.34	69.51
	✗	R50	BEVFormer	110	70.52	70.77	74.27	71.85	62.98	70.53	73.89	69.13	77.28

• AP_{ped.}, AP_{div.}, AP_{bou.} denote the Average Precision (AP) for pedestrian crossings, lane dividers, and road boundaries, respectively.

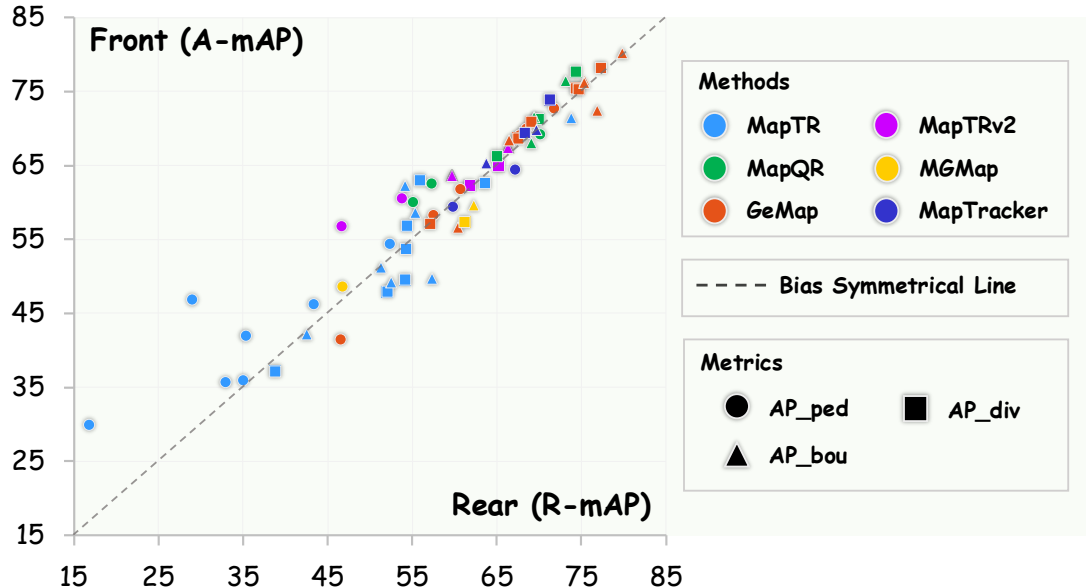


Figure 8. Front-Rear mAP Performance Benchmark for Single-Frame Models. Compared to temporal models, which rely on history aggregation, single-frame models exhibit a significantly reduced tendency toward rear performance bias. This is evident as the data points primarily cluster tightly around the y=x reference line, indicating similar performance regardless of the direction.

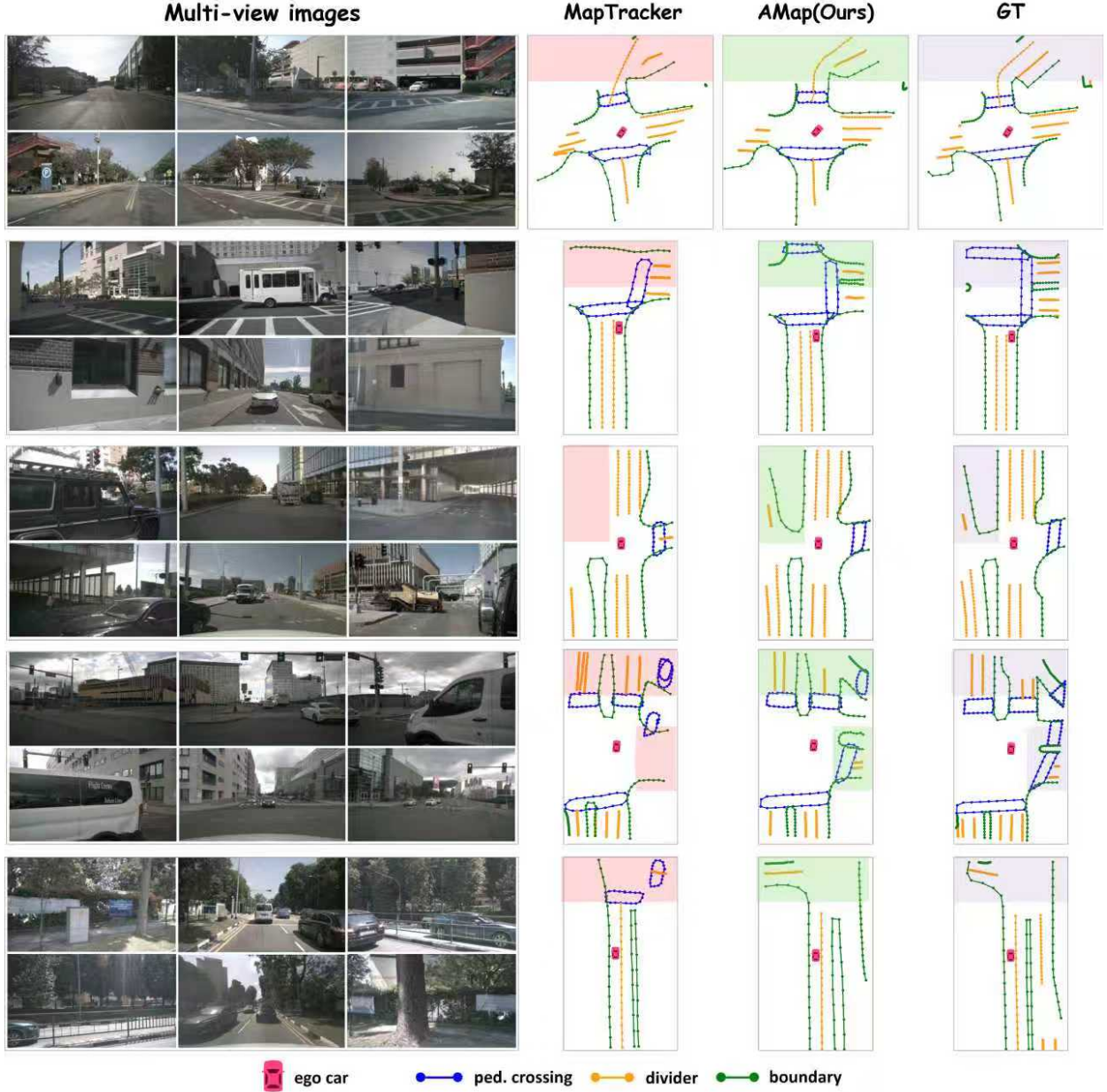


Figure 9. **Qualitative results on nuScenes dataset (Part 1).** From left to right: input multi-view images, MapTracker predictions, our predictions, and GT annotation. Each row corresponds to one sample. Shades of red and green are used to identify the differing and matching parts compared to the ground truth, which is represented by shade of violet.

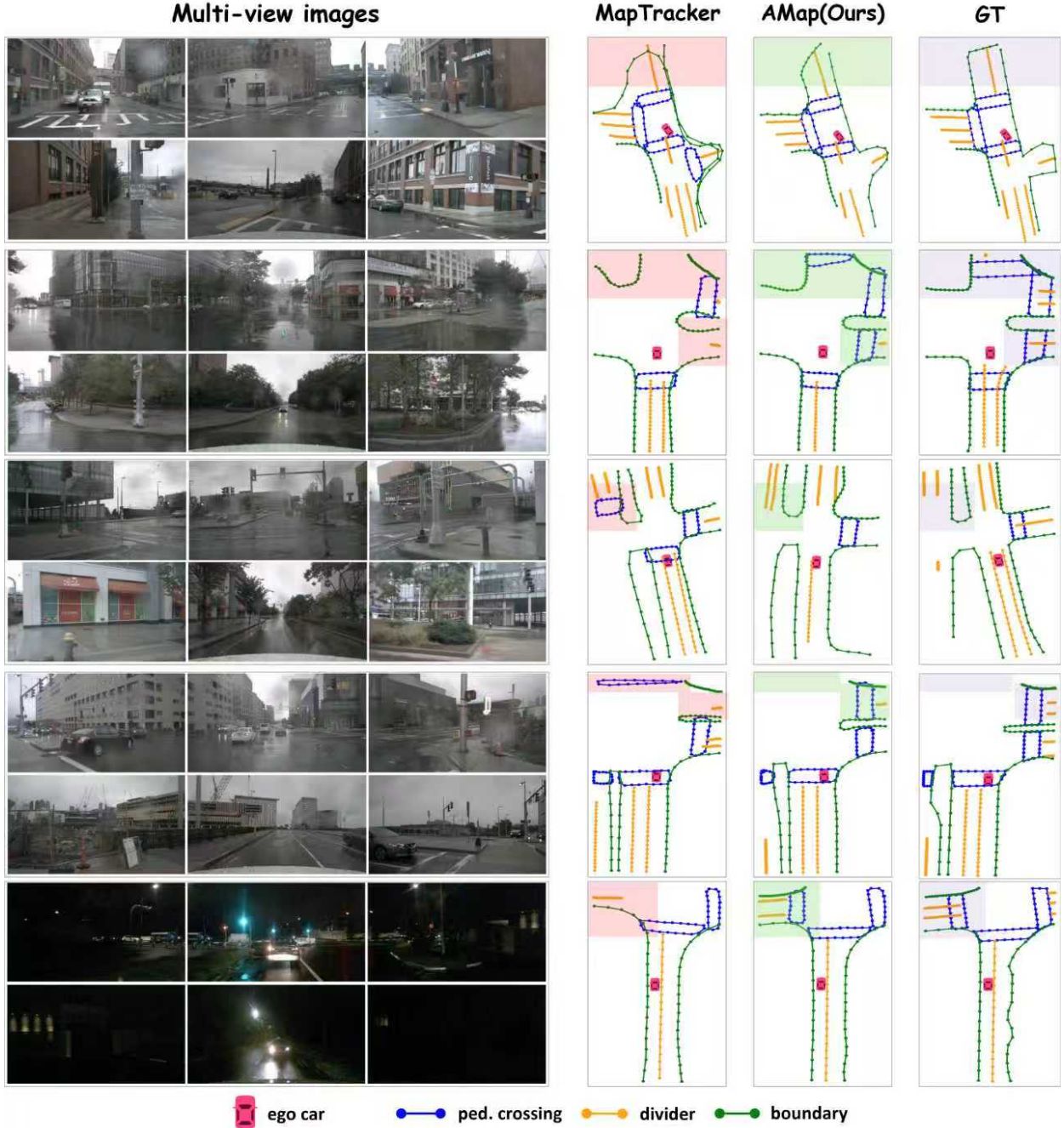


Figure 10. **Qualitative results on nuScenes dataset (Part 2).** From left to right: input multi-view images, MapTracker predictions, our predictions, and GT annotation. Each row corresponds to one sample. Shades of red and green are used to identify the differing and matching parts compared to the ground truth, which is represented by shade of violet. Our proposed AMap demonstrates outstanding performance under various weather and lighting conditions, particularly in capturing the complex topological structure of map elements.

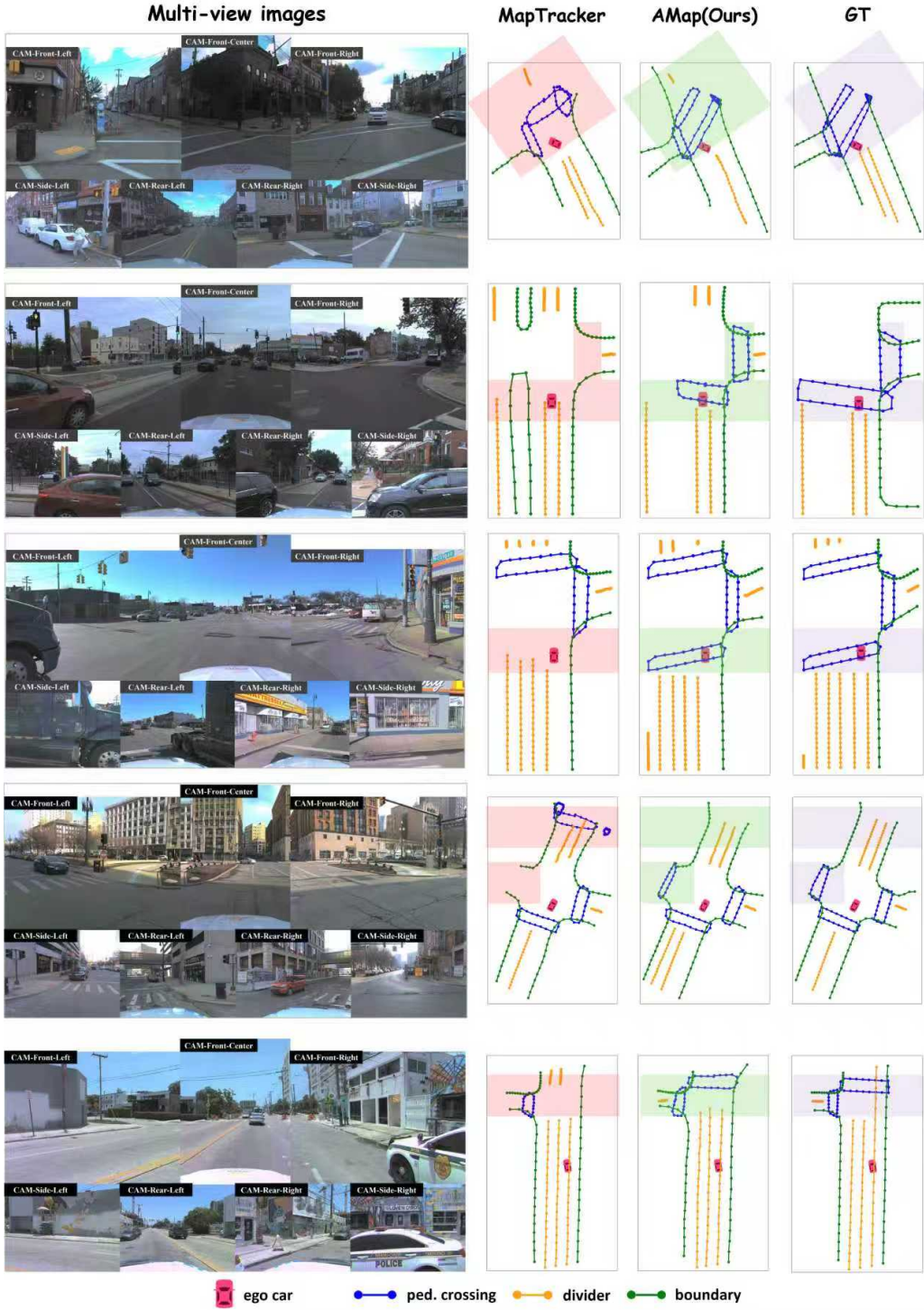


Figure 11. **Qualitative results on Argoverse 2 dataset.** From left to right: input multi-view images, MapTracker predictions, our predictions, and GT annotation. Each row corresponds to one sample. Shades of red and green are used to identify the differing and matching parts compared to the ground truth, which is represented by shade of violet.

References

[1] Holger Caesar, Varun Bankiti, Alex H Lang, Sourabh Vora, Venice Erin Liang, Qiang Xu, Anush Krishnan, Yu Pan, Gi-an-carlo Baldan, and Oscar Beijbom. nuscenes: A multi-modal dataset for autonomous driving. In *Proceedings of the IEEE/CVF conference on computer vision and pattern recognition*, pages 11621–11631, 2020. [2](#), [5](#), [6](#)

[2] Jiahao Chang, Shuo Wang, Hai-Ming Xu, Zehui Chen, Chenhongyi Yang, and Feng Zhao. Detrdistill: A universal knowledge distillation framework for detr-families. In *Proceedings of the IEEE/CVF international conference on computer vision*, pages 6898–6908, 2023. [5](#)

[3] Xinyuan Chang, Maixuan Xue, Xinran Liu, Zheng Pan, and Xing Wei. Driving by the rules: A benchmark for integrating traffic sign regulations into vectorized hd map. In *Proceedings of the Computer Vision and Pattern Recognition Conference*, pages 6823–6833, 2025. [2](#)

[4] Jiacheng Chen, Yuefan Wu, Jiaqi Tan, Hang Ma, and Yasutaka Furukawa. Maptracker: Tracking with strided memory fusion for consistent vector hd mapping. In *European Conference on Computer Vision*, pages 90–107. Springer, 2024. [2](#), [3](#), [4](#), [5](#), [6](#), [8](#)

[5] Zehui Chen, Zhenyu Li, Shiquan Zhang, Liangji Fang, Qin-hong Jiang, and Feng Zhao. Bevdistill: Cross-modal bev distillation for multi-view 3d object detection. *arXiv preprint arXiv:2211.09386*, 2022. [3](#), [5](#), [7](#)

[6] Wenjie Ding, Limeng Qiao, Xi Qiu, and Chi Zhang. Pivot-net: Vectorized pivot learning for end-to-end hd map construction. In *Proceedings of the IEEE/CVF International Conference on Computer Vision*, pages 3672–3682, 2023. [1](#), [2](#)

[7] Jinpeng Dong, Chen Li, Yutong Lin, Jingwen Fu, Sanping Zhou, and Nanning Zheng. Damap: Distance-aware mapnet for high quality hd map construction. In *Proceedings of the IEEE/CVF International Conference on Computer Vision*, pages 5285–5294, 2025. [2](#)

[8] Xiaoshuai Hao, Ruikai Li, Hui Zhang, Dingzhe Li, Rong Yin, Sangil Jung, Seung-In Park, ByungIn Yoo, Haimei Zhao, and Jing Zhang. Mapdistill: Boosting efficient camera-based hd map construction via camera-lidar fusion model distillation. In *European Conference on Computer Vision*, pages 166–183. Springer, 2024. [3](#), [5](#), [7](#), [8](#)

[9] Xiaoshuai Hao, Mengchuan Wei, Yifan Yang, Haimei Zhao, Hui Zhang, Yi Zhou, Qiang Wang, Weiming Li, Lingdong Kong, and Jing Zhang. Is your hd map constructor reliable under sensor corruptions? *Advances in Neural Information Processing Systems*, 37:22441–22482, 2024. [2](#)

[10] Xiaoshuai Hao, Lingdong Kong, Rong Yin, Pengwei Wang, Jing Zhang, Yunfeng Diao, and Shu Zhao. Safemap: Robust hd map construction from incomplete observations. *arXiv preprint arXiv:2507.00861*, 2025. [3](#)

[11] Kaiming He, Xiangyu Zhang, Shaoqing Ren, and Jian Sun. Deep residual learning for image recognition. In *Proceedings of the IEEE conference on computer vision and pattern recognition*, pages 770–778, 2016. [2](#)

[12] Junjie Huang and Guan Huang. Bevdet4d: Exploit tempo-
ral cues in multi-camera 3d object detection. *arXiv preprint arXiv:2203.17054*, 2022. [3](#)

[13] Zhou Jiang, Zhenxin Zhu, Pengfei Li, Huan-ang Gao, Tianyuan Yuan, Yongliang Shi, Hang Zhao, and Hao Zhao. P-mapnet: Far-seeing map generator enhanced by both sdmap and hdmap priors. *IEEE Robotics and Automation Letters*, 2024. [2](#)

[14] Kang Ke, Haonan Zhang, Yuqi Huang, Penghui Fan, and Longjun Liu. Efficient vision-based occupancy prediction with knowledge distillation. *Pattern Recognition*, page 112631, 2025. [3](#)

[15] Donghyeon Kwon, Youngseok Yoon, Hyeongseok Son, and Suha Kwak. Memdistill: Distilling lidar knowledge into memory for camera-only 3d object detection. In *Proceedings of the IEEE/CVF International Conference on Computer Vision*, pages 6828–6838, 2025. [3](#)

[16] Bohan Li, Xin Jin, Jianan Wang, Yukai Shi, Yasheng Sun, Xiaofeng Wang, Zhuang Ma, Bao Xie, Chao Ma, Xiaokang Yang, et al. Occscene: Semantic occupancy-based cross-task mutual learning for 3d scene generation. *IEEE Transactions on Pattern Analysis and Machine Intelligence*, 2025. [3](#)

[17] Bohan Li, Xin Jin, Hu Zhu, Hongsi Liu, Ruikai Li, Jia-
zhe Guo, Kaiwen Cai, Chao Ma, Yueming Jin, Hao Zhao, et al. Scaling up occupancy-centric driving scene generation: Dataset and method. *arXiv preprint arXiv:2510.22973*, 2025. [3](#)

[18] Qi Li, Yue Wang, Yilun Wang, and Hang Zhao. Hdmapnet: An online hd map construction and evaluation framework. In *2022 International Conference on Robotics and Automation (ICRA)*, pages 4628–4634. IEEE, 2022. [1](#), [2](#)

[19] Siyu Li, Jiacheng Lin, Hao Shi, Jiaming Zhang, Song Wang, You Yao, Zhiyong Li, and Kailun Yang. DtclmMapper: Dual temporal consistent learning for vectorized hd map construction. *IEEE Transactions on Intelligent Transportation Systems*, 2024. [2](#)

[20] Yang Li, Zongzheng Zhang, Xuchong Qiu, Xinrun Li, Ziming Liu, Leichen Wang, Ruikai Li, Zhenxin Zhu, Huan-ang Gao, Xiaojian Lin, et al. Reusing attention for one-stage lane topology understanding. *arXiv preprint arXiv:2507.17617*, 2025. [3](#)

[21] Zhiqi Li, Wenhui Wang, Hongyang Li, Enze Xie, Chong-hao Sima, Tong Lu, Qiao Yu, and Jifeng Dai. Bevformer: learning bird’s-eye-view representation from lidar-camera via spatiotemporal transformers. *IEEE Transactions on Pattern Analysis and Machine Intelligence*, 2024. [3](#), [5](#)

[22] Bencheng Liao, Shaoyu Chen, Xinggang Wang, Tianheng Cheng, Qian Zhang, Wenyu Liu, and Chang Huang. Maptr: Structured modeling and learning for online vectorized hd map construction. *arXiv preprint arXiv:2208.14437*, 2022. [2](#), [3](#), [6](#), [7](#), [1](#)

[23] Bencheng Liao, Shaoyu Chen, Yunchi Zhang, Bo Jiang, Qian Zhang, Wenyu Liu, Chang Huang, and Xinggang Wang. Maptrv2: An end-to-end framework for online vectorized hd map construction. *International Journal of Computer Vision*, 133(3):1352–1374, 2025. [1](#), [2](#), [7](#), [3](#)

[24] Adam Lilja, Erik Wallin, Junsheng Fu, and Lars Hammarstrand. Exploring semi-supervised learning for online

mapping. In *Proceedings of the Computer Vision and Pattern Recognition Conference*, pages 2477–2487, 2025. 3

[25] Xiaolu Liu, Song Wang, Wentong Li, Ruizi Yang, Junbo Chen, and Jianke Zhu. Mgmap: Mask-guided learning for online vectorized hd map construction. In *Proceedings of the IEEE/CVF Conference on Computer Vision and Pattern Recognition*, pages 14812–14821, 2024. 1, 2, 7, 3

[26] Xiaolu Liu, Ruizi Yang, Song Wang, Wentong Li, Junbo Chen, and Jianke Zhu. Uncertainty-instructed structure injection for generalizable hd map construction. In *Proceedings of the Computer Vision and Pattern Recognition Conference*, pages 22359–22368, 2025.

[27] Yicheng Liu, Tianyuan Yuan, Yue Wang, Yilun Wang, and Hang Zhao. Vectormapnet: End-to-end vectorized hd map learning. In *International Conference on Machine Learning*, pages 22352–22369. PMLR, 2023. 1, 2

[28] Zhijian Liu, Haotian Tang, Alexander Amini, Xinyu Yang, Huizi Mao, Daniela Rus, and Song Han. Bevfusion: Multi-task multi-sensor fusion with unified bird’s-eye view representation. *arXiv preprint arXiv:2205.13542*, 2022. 2

[29] Zihao Liu, Xiaoyu Zhang, Guangwei Liu, Ji Zhao, and Ningyi Xu. Leveraging enhanced queries of point sets for vectorized map construction. In *European Conference on Computer Vision*, pages 461–477. Springer, 2024. 1, 2, 7, 3

[30] Ilya Loshchilov and Frank Hutter. Decoupled weight decay regularization. *arXiv preprint arXiv:1711.05101*, 2017. 6

[31] Jonah Philion and Sanja Fidler. Lift, splat, shoot: Encoding images from arbitrary camera rigs by implicitly unprojecting to 3d. In *European conference on computer vision*, pages 194–210. Springer, 2020. 2

[32] Limeng Qiao, Wenjie Ding, Xi Qiu, and Chi Zhang. End-to-end vectorized hd-map construction with piecewise bezier curve. In *Proceedings of the IEEE/CVF Conference on Computer Vision and Pattern Recognition*, pages 13218–13228, 2023. 1

[33] Shoumeng Qiu, Xinrun Li, Yang Long, Xiangyang Xue, Varun Ojha, and Jian Pu. Learning global representation from queries for vectorized hd map construction. *arXiv preprint arXiv:2510.06969*, 2025. 2

[34] Hao Shan, Ruihai Li, Han Jiang, Yizhe Fan, Ziyang Yan, Bohan Li, Xiaoshuai Hao, Hao Zhao, Zhiyong Cui, Yilong Ren, et al. Stability under scrutiny: Benchmarking representation paradigms for online hd mapping. *arXiv preprint arXiv:2510.10660*, 2025.

[35] Jiaxu Wan, Xu Wang, Mengwei Xie, Xinyuan Chang, Xinran Liu, Zheng Pan, Mu Xu, and Ding Yuan. Driving by hybrid navigation: An online hd-sd map association framework and benchmark for autonomous vehicles. *arXiv preprint arXiv:2507.07487*, 2025.

[36] Jiaxu Wan, Hong Zhang, Ziqi He, Yangyan Deng, Qishu Wang, Ding Yuan, and Yifan Yang. Sp2t: Sparse proxy attention for dual-stream point transformer. In *Proceedings of the IEEE/CVF International Conference on Computer Vision*, pages 27885–27895, 2025. 2

[37] Xiaofeng Wang, Zheng Zhu, Guan Huang, Xinze Chen, Jia-gang Zhu, and Jiwen Lu. Drivedreamer: Towards real-world-drive world models for autonomous driving. In *European conference on computer vision*, pages 55–72. Springer, 2024. 3

[38] Benjamin Wilson, William Qi, Tanmay Agarwal, John Lambert, Jagjeet Singh, Siddhesh Khandelwal, Bowen Pan, Ratnesh Kumar, Andrew Hartnett, Jhony Kaesemeyer Pontes, et al. Argoverse 2: Next generation datasets for self-driving perception and forecasting. *arXiv preprint arXiv:2301.00493*, 2023. 2, 5, 7

[39] Kuang Wu, Chuan Yang, and Zhanbin Li. Interactionmap: Improving online vectorized hdmap construction with interaction. In *Proceedings of the Computer Vision and Pattern Recognition Conference*, pages 17176–17186, 2025. 2

[40] Mengwei Xie, Shuang Zeng, Xinyuan Chang, Xinran Liu, Zheng Pan, Mu Xu, and Xing Wei. Seqgrowgraph: Learning lane topology as a chain of graph expansions. In *Proceedings of the IEEE/CVF International Conference on Computer Vision*, pages 27166–27175, 2025.

[41] Ziyang Yan, Ruihai Li, Zhiyong Cui, Bohan Li, Han Jiang, Yilong Ren, Aoyong Li, Zhenning Li, Sijia Wen, and Haiyang Yu. Mapkd: Unlocking prior knowledge with cross-modal distillation for efficient online hd map construction. *arXiv preprint arXiv:2508.15653*, 2025. 2

[42] Jing Yang, Sen Yang, Xiao Tan, and Hanli Wang. His-trackmap: Global vectorized high-definition map construction via history map tracking. *arXiv preprint arXiv:2503.07168*, 2025. 2

[43] Tianyuan Yuan, Yicheng Liu, Yue Wang, Yilun Wang, and Hang Zhao. Streammapnet: Streaming mapping network for vectorized online hd map construction. In *Proceedings of the IEEE/CVF Winter Conference on Applications of Computer Vision*, pages 7356–7365, 2024. 2, 3, 6

[44] Yujian Yuan, Changjie Wu, Xinyuan Chang, Sijin Wang, Hang Zhang, Shiyi Liang, Shuang Zeng, Mu Xu, and Ning Guo. Unimapgen: A generative framework for large-scale map construction from multi-modal data. *arXiv preprint arXiv:2509.22262*, 2025. 2

[45] Gongjie Zhang, Jiahao Lin, Shuang Wu, Zhipeng Luo, Yang Xue, Shijian Lu, Zuoguan Wang, et al. Online map vectorization for autonomous driving: A rasterization perspective. *Advances in Neural Information Processing Systems*, 36:31865–31877, 2023. 1, 2

[46] Haiming Zhang, Xu Yan, Dongfeng Bai, Jiantao Gao, Pan Wang, Bingbing Liu, Shuguang Cui, and Zhen Li. Radocc: Learning cross-modality occupancy knowledge through rendering assisted distillation. In *Proceedings of the AAAI Conference on Artificial Intelligence*, pages 7060–7068, 2024. 3

[47] Xiaoyu Zhang, Guangwei Liu, Zihao Liu, Ningyi Xu, Yun-hui Liu, and Ji Zhao. Enhancing vectorized map perception with historical rasterized maps. In *European Conference on Computer Vision*, pages 422–439. Springer, 2024. 2, 6

[48] Zhixin Zhang, Yiyuan Zhang, Xiaohan Ding, Fusheng Jin, and Xiangyu Yue. Online vectorized hd map construction using geometry. In *European Conference on Computer Vision*, pages 73–90. Springer, 2024. 1, 2, 7, 3

[49] Zongzheng Zhang, Xuchong Qiu, Boran Zhang, Guantian Zheng, Xunjiang Gu, Guoxuan Chi, Huan-ang Gao, Leichen Wang, Ziming Liu, Xinrun Li, et al. Delving into mapping

uncertainty for mapless trajectory prediction. *arXiv preprint arXiv:2507.18498*, 2025. 3, 1

[50] Haimei Zhao, Qiming Zhang, Shanshan Zhao, Zhe Chen, Jing Zhang, and Dacheng Tao. Simdistill: Simulated multi-modal distillation for bev 3d object detection. In *Proceedings of the AAAI conference on artificial intelligence*, pages 7460–7468, 2024. 3

[51] Shengchao Zhou, Weizhou Liu, Chen Hu, Shuchang Zhou, and Chao Ma. Unidistill: A universal cross-modality knowledge distillation framework for 3d object detection in bird’s-eye view. In *Proceedings of the IEEE/CVF conference on computer vision and pattern recognition*, pages 5116–5125, 2023. 3

[52] Zikang Zhou, Luyao Ye, Jianping Wang, Kui Wu, and Kejie Lu. Hivt: Hierarchical vector transformer for multi-agent motion prediction. In *Proceedings of the IEEE/CVF conference on computer vision and pattern recognition*, pages 8823–8833, 2022. 4, 1